Effect of cerium, lanthanum and thorium as alloying elements on the corrosion behavior of tungsten in 3.5 wt. % NaCl solution

L. Díaz-Ballote [*, a], V. Rejón [a], L. Maldonado [a], M. Alpuche [b], T. Vega-Lizama [a]

[a] Department of Applied Physics, CINVESTAV-Merida, km 6 ant. carr. a Progreso, Mérida, Yucatán, 97310, México

[b] Department of Chemistry, University of Nevada, Reno, NV 89557, USA

* Corresponding Author: L. Díaz-Ballote (luisdiaz@cinvestav.mx)

Abstract

Tungsten is a refractory metal with unique physical and chemical properties that have well recognized applications at high temperatures. At room temperature it has been proposed for medical applications such as microelectrodes or implants, due to its protection by an oxide/hydroxide film. However, oxide films breakdown and tungsten dissolution issues are of great concern because of their potential adverse effects on human health. In the present study, the corrosion of tungsten with and without rare-earth elements (Th, Ce, and La) was investigated using electrochemical techniques such as open circuit potential (OCP), potentiodynamic polarization, and electrochemical impedance spectroscopy (EIS). As a first approach, a 3 wt.% NaCl solution was used as the corrosive media. The polarization curves are consistent with the presence of an oxide film, likely WO_3, followed by tungsten dissolution. X-ray photoelectron spectroscopy (XPS) confirmed the presence of WO_3 on the surface of tungsten and tungsten alloys. This tungsten oxide also had minor content of rare-earth element oxides. Although the tungsten behavior dominated corrosion, it was seen that lanthanum and Cerium could be candidates to decrease the corrosion rate of tungsten. On the other hand, thorium/tungsten alloy has similar corrosion rates to tungsten. From a corrosion point of view, the results suggest that Ce or La could replace Th, in tungsten/rare earth elements alloys which is less attractive because of Th radioactive nature.

Keywords: rare earth elements; corrosion; tungsten; NaCl solution

Introduction

Tungsten is an attractive material due to its remarkable physical and chemical properties. This refractory metal has a melting point of 3,422 °C, [1] the highest melting point of metals. It is highly resistant to heat and wear. It is also considered an inert metal with high corrosion resistance. In addition, it possesses an extremely high density of 19.3 g cm^{-3} [2]. For that reason, tungsten has various end uses, typically tungsten is used to produce reactors, tools, machinery, welding electrodes, and casting molds [2,3]. Tungsten has also found applications in the health field as a microelectrode for electrochemical measurements in the brain [4] and in medical implants [4,5]. Tungsten coil was assessed in vitro by Peuster *et al.* [6] using Ringer´s solution. The authors reported a low corrosion rate of tungsten and discarded its potential toxicity because they found a low concentration of dissolved metal ions. Although tungsten has been considered chemically inert, Patrick *et al*. [7] studied tungsten corrosion in biological saline environments. They found that tungsten undergoes oxidation to tungstic ions without forming a stable film. Idil *et al*. [8] reviewed tungsten as an implant material. The authors concluded that tungsten has a poor corrosion resistance in aqueous solution and that pure tungsten is unsuitable as a chronic implant material. The authors state that W does not have a noble surface or a stable passive film of WO_3. They say that at the ordinary body's pH, the oxide dissolves to W^{+6} commonly represented by WO_4^{2-}. On the other hand, alloying is a well-known method to improve metals´ mechanical and chemical properties. Tungsten alloys are typically fabricated by mechanical alloying where contaminants such as oxides, nitrated and carbides are undesirable species that can produce embrittlement of the alloys. Rare-earth elements with higher affinity to oxygen than tungsten are added as alloying elements to trap the oxygen during the alloying process and reduce the formation of impurities [9]. Another role of rare elements is to promote a reduction in the grain size in electrodes for the tungsten inert gas (TIG) welding process [10]. Anti-corrosive coatings have also been produced with rare-earth elements to protect metals or alloys. Lanthanum, for example, has been used to improve the corrosion resistance of aluminum alloy 6061-T6 [11]. Magnesium alloy AZ91D has increased its corrosion resistance using a cerium coating [12]. However, few studies have been performed on the aqueous corrosion behavior of tungsten-containing rare earth elements as alloying elements. Rare-earth alloyed tungsten provides an excellent opportunity to gain more insight into the corrosion behavior of tungsten. As a first approach in the present work, the main aim was to investigate the effect of rare earth elements (Ce, La, and Th) as alloying elements of tungsten in a 3.5 wt. % NaCl solution. Open circuit potential (OCP), electrochemical impedance spectroscopy (EIS), and potentiodynamic polarization were used to assess the corrosion performance of rare-earth elements as alloying elements for tungsten.

Materials and methods

Rods (3/32 dia.) of commercial tungsten (~99.95 wt.%, coded W-P) and tungsten with rare earth elements (nominal content 2% wt.) were purchased via Amazon. Samples of tungsten W-P and its

alloys; tungsten with lanthanum (coded W-2La), tungsten with cerium (coded W-2Ce), and tungsten with thorium (coded W-2Th) were embedded in epoxy resin. Then, the samples were successively abraded using 600, 800, 1500, and 2000 grit SiC-paper. Deionized water was used between each successively finer grade of SiC paper to remove debris. The rare-earth compound dispersion and elemental composition were investigated with an FE-SEM microscope in secondary electron (SEI) and low-angle backscattering electron (LABE). EDAX spectra of tungsten and its alloys were also acquired. Surface analysis of tungsten and tungsten/rare-earth elements was conducted using a Thermo Scientific X-ray photoelectron spectrometer (XPS) with monochromatic Al K-alpha radiation (1486.6 eV). The XPS spectra were then deconvoluted into components using the computer software XPSPeak version 4.1 (freeware written by Raymond Kwok, Hong Kong, China). The solution of 3.5 wt. % NaCl (pH 6.8) was prepared with 7 g of NaCl reagent grade bought from Sigma Aldrich and 193 mL of deionized water. The effect of rare earth elements on the corrosion resistance of tungsten was evaluated with a Gamry Instruments Reference 600 potentiostat. The working electrode (tungsten sample) was immersed in a classical three-electrode cell having platinum foil as an auxiliary electrode (AE) and a calomel reference electrode (SCE). The open circuit potential (OCP) was monitored for 5400 s to gain insight into the system stability. Following the OCP measurements, impedance measurements or polarization measurements were carried out. Polarization was performed by scanning the potential of the working electrode from -300 mV to 300 mV from the OCP at a rate of 5 mV/s. The impedance spectra were acquired from 100 kHz to 0.01 Hz with a signal amplitude of 7 mV.

Experimental results and discussion

Figure 1 shows FE-SEM image in LABE mode of tungsten (W-P). The surface seems to be relatively free of flaws and pores. The lines observed came from the polishing process.

Figure 2 shows FE-SEM images in the SEI and LABE modes of tungsten alloys W-2Ce, W-2Th, and W-2La. The low energy of secondary electrons (SEI images) makes them suitable for studying the surface morphology of the sample. Then, the SEI images suggest that a few small defects, such as pores, are present on the surface. In contrast, LABE images are more sensitive to the molecular weight of elements. Tungsten has a higher molecular weight than the rare-earth elements. Therefore, tungsten is expected to appear brighter than rare earth elements. Considering the images in LABE mode, it is possible to see a homogeneous distribution of rare-earth compounds (Ce, Th, and La) in the tungsten matrix. The chemical composition of tungsten alloys was confirmed with EDAX analysis. Table 1 compares the nominal content and the content measured from EDAX. All alloys have a composition close to the nominal composition, confirming the presence of rare-earth element in the alloys.

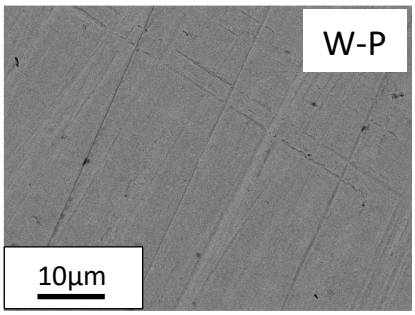

Figure 1. FE-SEM LABE (low angle backscattered electron image) for tungsten (W-P).

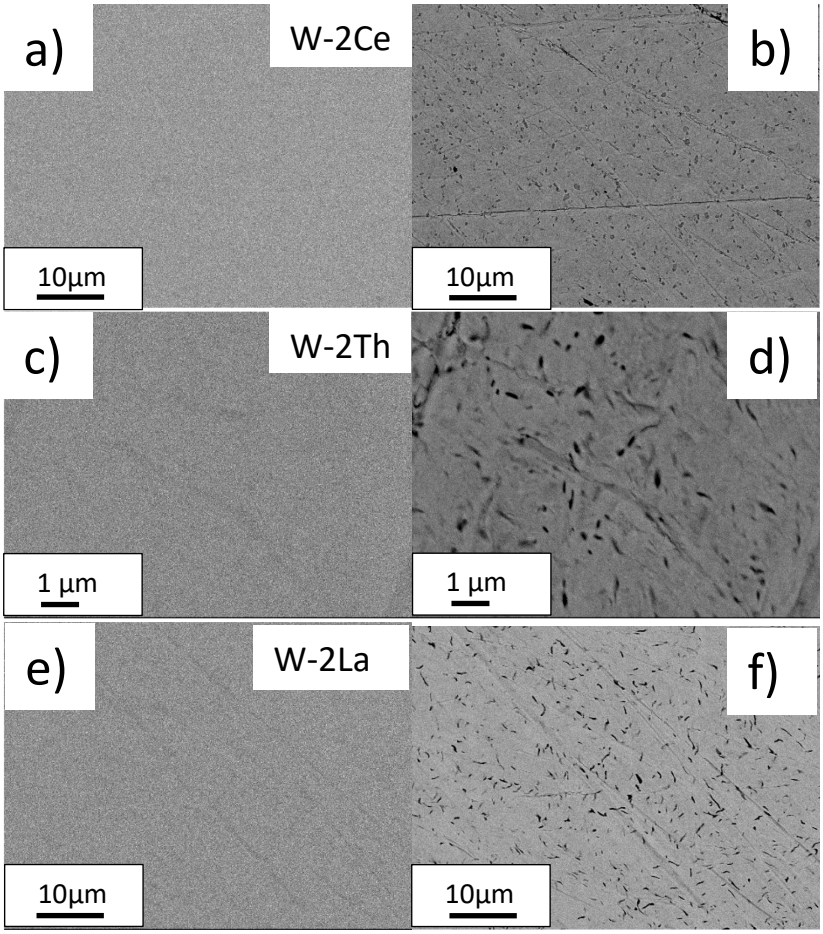

Figure 2. FE-SEM SEI (secondary detector electron image) and FE-SEM LABE (low angle backscattered electron image) for rare-earth tungsten alloys; micrographs a and b for W-2Ce, micrographs c and d for W-2Th, and micrographs e and f for W-2La respectively.

Table 1. Chemical composition of tungsten alloys

Nominal content (% wt.)	Measured content from EDAX (% wt.)

W-P	0.05<
W-2% Ce	2.09
W-2% La	1.82
W-2% Th	1.73

Pourbaix diagram of tungsten

The Pourbaix diagram of tungsten [13] is shown in Figure 3. The dashed lines represent the region of water stability. From the Pourbaix diagram, a protective layer formation is expected to protect the tungsten surface up to pH=5. At higher pH values, the protective layer (likely WO_3) will form tungstic ions (Equation (1)) [14,15].

$$WO_3 + H_2O \rightarrow WO_4^{2-} + 2H^+ \quad (1)$$

The dissolution of WO_3 will accelerate the corrosion process of tungsten through the reaction given by Equation (2),

$$W + 4H_2O \rightarrow WO_4^{2-} + 8H^+ + 6e^- \quad (2)$$

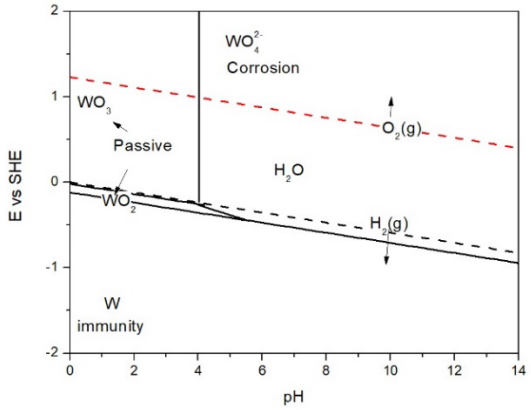

Figure 3. Pourbaix diagram of the W-H_2O system (metal ion concentration of 10^{-6}) [13].

Electrochemical measurements

Open circuit potential measurements

The electrochemical system should be stable during most electrochemical tests. Therefore, we monitored the open circuit potential to gain insight into the system stability and determine the delay time before the impedance and potentiodynamic measurements. Figure 4 shows the open circuit potential as a function of time for tungsten and tungsten alloys. Tungsten and its alloys shift the potential in the positive direction. In other words, all alloys become more noble as a function of time. These results agree with the forming of an oxide film that is most likely to be WO_3. The W-2La shows a higher positive value. Below W-2La are W-2Ce, W-2Th, and W-P.

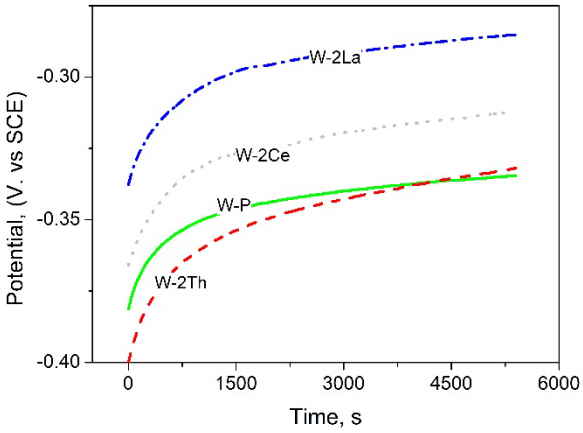

Figure 4. Open circuit potential of tungsten (W-P) and rare-earth added tungsten (W-2Ce, W-2Th, and W-2La).

Potentiodynamic polarization

After the open circuit potential measurement, potentiodynamic polarization was carried out. Figure 5 shows typical polarization curves for tungsten and tungsten alloys. The cathodic branch of the polarization curves shows a similar slope, showing that the reduction reaction is the same in all alloys. Therefore, the most likely reduction reaction in a neutral NaCl solution is mainly that of dissolved oxygen represented by Equation (3) [16].

$$O_2 + 2H_2O + 4e^- \rightarrow 4OH^- \quad (3)$$

The anodic branch of the polarization curve shows an unstable film formation that sometimes was not present, as seen in the polarization curve of W-P. At higher anodic overpotentials, the slopes for tungsten and alloys are also similar. This result suggests that the anodic reaction at a higher overpotential is the same as that for pure tungsten. A linear anodic region is not present due to the passivation effect. Therefore, Tafel analysis using the anodic and cathodic branches of the polarization curves is not possible. However, as noted by McCafferty [16], an alternative is to use only the cathodic branch, and the results can be useful for comparing the corrosion parameters. Table 2 shows the average corrosion parameters from at least five replicated tests, considering

only the cathodic branch of the polarization curves. The corrosion potentials of tungsten and its alloys were found to be similar. On the other hand, a slight difference was seen in the corrosion current of all samples. Although a slight difference in the corrosion current density was found, the predominant corrosion properties are clearly due to tungsten. Therefore, the rare-earth concentration in the tungsten alloy (2% wt.) caused a small effect on the corrosion properties of tungsten for Th, while the samples of Ce and La have a passive region suggesting their usefulness in decreasing the corrosion rate of W alloys.

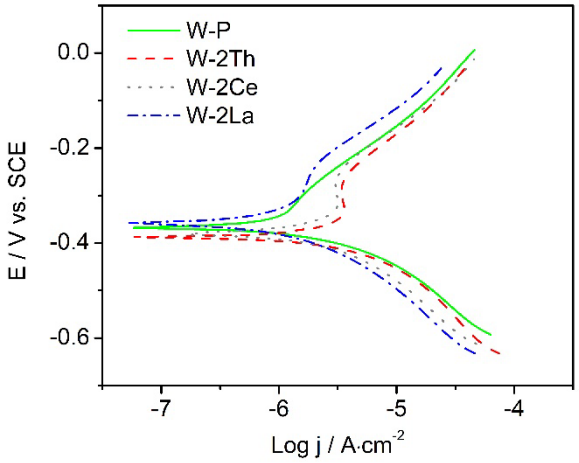

Figure 5. Typical polarization curves of tungsten (W-P) and rare-earth added tungsten (W-2Ce, W-2Th, and W-2La).

The average corrosion current grows in the order W-2La > W-2Ce > W-2Th > W-P, agrees with the activity of the samples derived from the open circuit potential in Figure 4. The Tafel slope of the cathodic branch looks similar in Figure 5, and the average cathodic Tafel slope in Table 2 suggests that the reduction reaction is the same. The cathodic slope looks higher than the typical value of 0.120 mV decade^{-1} reported for oxygen reduction in a similar NaCl solution. However, it must be considered that the oxygen reduction reaction probably takes place on an oxide/hydroxide film of WO_3.

Table 2. Average corrosion parameters from at least five replicated polarization curves

Alloy	E_{corr} (mV vs SCE)	i_{corr} (μA cm^{-2})	b_c (mV decade^{-1})
W-2La	-350.0±10.4	3.3±1.4	216.0±0.1
W-2Ce	-381.0±17.3	4.6±1.0	213.0±0.1
W-2Th	-404.0±15.6	5.1±1.8	218.0±0.1
W-P	-378.0±8.7	5.1±0.4	233.0±0.1

Error values correspond to ±1σ.

Electrochemical impedance spectroscopy

Figure 6 shows representative Nyquist and Bode plots of tungsten and tungsten alloys immersed in 3.5 wt. % NaCl. The experimental data were modeled with the equivalent circuit in Figure 7, [17], where R_s, R_f, and R_{ct} are the solution, film, and charge transfer resistances, respectively. Q_{dl} and Q_f are the double layer and film constant-phase elements (CPEs). The experimental impedance spectra do not show ideal semicircles, ascribed to the frequency dispersion effect; constant phase elements (CPEs) were used to model the deviation from an ideal capacitor [18]. The constant phase element is characterized by two parameters, the admittance Y_0 in units of $s^n\ \Omega^{-1}$ and the exponent "n". For comparison, an ideal capacitance has s Ω^{-1} or F [19]. Evidently, when n=1, the CPE (constant phase elements) behaves like an ideal capacitor. Commonly, the CPE is ascribed to surface inhomogeneities such as roughness and porosity. This equivalent circuit is frequently used to model a coating or a protective oxide film [17,20]. Figures 6 (a)-(b) show a slight difference between the impedance spectra of tungsten and tungsten alloy, confirming the small effect of rare-earth elements in the alloy. Although the impedance spectra are similar, is observed an increase in the semicircle diameter in the order W-P < W-2Th < W-2Ce < W-2La. Table 3 shows the average values of the impedance parameters obtained by modeling the experimental data using the equivalent circuit mentioned above (Figure 7). The charge transfer is inversely proportional to the corrosion rate. From Table 3, it is observed that W-2La possesses the largest R_{ct} or the lowest corrosion rate. This result agrees with the polarization results. Therefore, the addition of lanthanum slightly increases the corrosion resistance of tungsten.

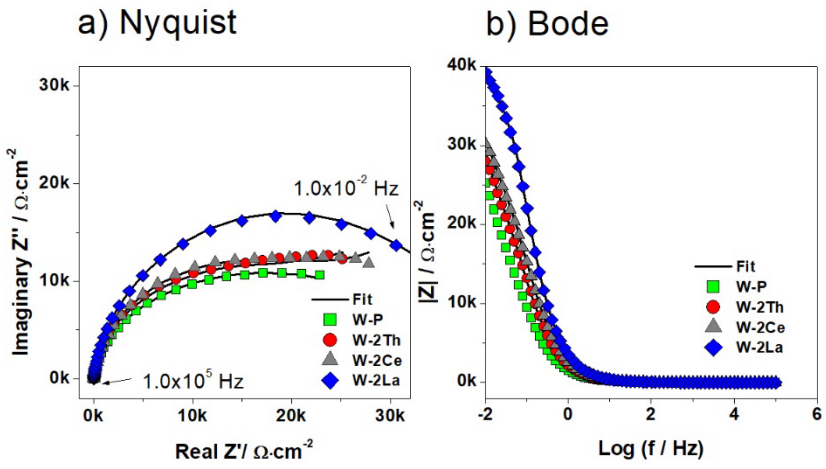

Figure 6. Representative EIS data of tungsten (W-P) and rare-earth added tungsten (W-2Ce, W-2Th, and W-2La): a) Nyquist plots, and b) Bode plots. Symbols are experimental data, and solid lines represent the fitted curve.

R_f and R_s remain almost constant, and these results can be explained by the presence of a native oxide with a similar thickness and the use of a solution with the same NaCl concentration.

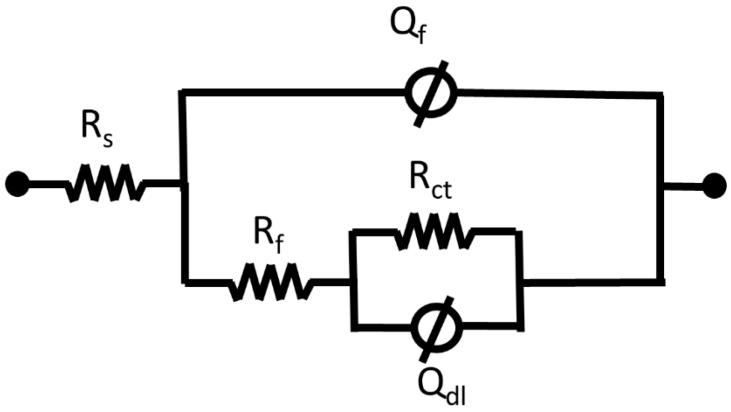

Figure 7. Equivalent circuit used for modeling the experimental impedance data.

The relatively similar values of Q_f also suggest the presence of the oxide film, with few inhomogeneities. In brief, the presence of an oxide film likely of WO_3 on tungsten was observed by polarization resistance as well as its dissolution at higher overpotentials. Impedance data confirm the presence of an oxide film and the slight improvement of tungsten corrosion resistance with lanthanum and Cerium. Note that because of the error of the measurements, Rct values for the La and Ce alloys could be considered equivalents. On the other hand, the corrosion resistance of W-2Th was found to be like corrosion resistance of tungsten.

Table 3. Average impedance parameters for corrosion of tungsten and tungsten alloys immersed in 3.5 wt.% NaCl (pH 6.8).

Alloy	R_{ct}	R_f	Q_{dl}		R_s	Q_f	
			Y_0	n		Y_0	m
	$\Omega \cdot cm^2$	$\Omega \cdot cm^2$	$S \cdot s^n \cdot cm^{-2}$		$\Omega \cdot cm^2$	$S \cdot s^n \cdot cm^{-2}$	
W-P	(2.8±1.0) x 10^{+4}	(2.1±0.5) x 10^{+4}	(4.9±4.4) x 10^{-4}	0.76±0.01	2.1±0.1	(1.1±0.1) x 10^{-4}	9.1±0.1
W-2Th	(3.1±0.8) x 10^{+4}	(1.7±0.7) x 10^{+4}	(5.7±1.1) x 10^{-4}	0.86±0.02	2.2±0.1	(1.1±0.1) x 10^{-4}	9.1±0.1
W-2Ce	(2.5±1.2) x 10^{+5}	(2.7±0.4) x 10^{+4}	(2.8±0.5) x 10^{-4}	0.53±0.08	2.2±0.2	(6.8±0.5) x 10^{-5}	9.1±0.1
W-2La	(6.0±4.2) x 10^{+5}	(3.4±0.3) x 10^{+4}	(2.8±5.5) x 10^{-2}	0.33±0.45	2.6±0.3	(8.6±3.0) x 10^{-5}	9.0±0.1

Error values correspond to ±1σ of at least 5 measurements.

EIS data validation

Electrochemical impedance spectroscopy is fundamentally based on linear system theory. Therefore, the experimental data must satisfy the conditions for a linear system, such as linearity, causality, and stability. Kramer-Kronig (KK) transformations were used to validate that the experimental data met the conditions for a linear system. These mathematical relations are used to calculate the imaginary part from the experimental real part of impedance and vice versa. The residual error between the calculated and experimental impedance data is used to evaluate the linear behavior of the electrochemical system. The Chem Analyst software from Gamry instrument has implemented the Kramer-Kronig analysis in agreement with the procedure described by Boukamp [21]. This software was used to determine if the electrochemical system behaves as a linear system. The Nyquist plot (Figure 8(a)) and Bode plot (Figure 8(b)) show the experimental data and the corresponding Kramer-Kronig fit. Figures 8(a)-(b), show a good fit. Figure 8(c) shows the residual error for both imaginary and real parts; the residual error for both parts is <0.4%. The maximum residual error found for W-alloys was also good (<0.6%) [22].

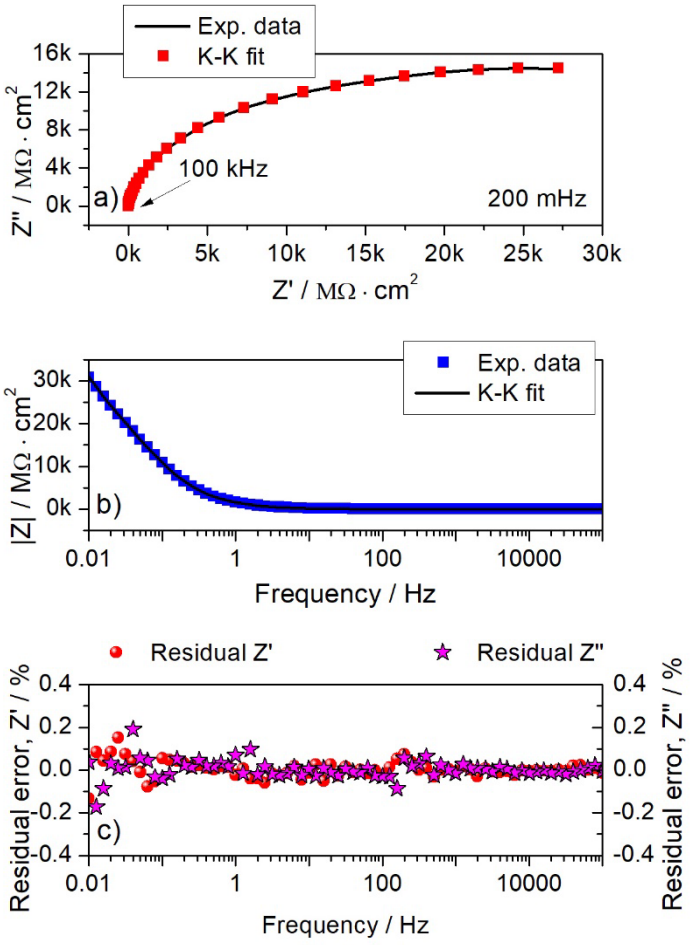

Figure 8. Experimental Nyquist (a) and Bode (b) curves of tungsten in 3.5 wt.% NaCl (pH 6.8) and the Kramers-Kronig fit (solid line). The corresponding residual variations are also displayed in Figure (c).

Surface analysis of tungsten

Tungsten: The high-resolution XPS spectra of tungsten exposed to a 3.5 wt.% NaCl solution are shown in Figure 9(a). Four peaks reveal the presence of metallic tungsten and tungsten oxide. The presence of metallic tungsten is determined by two peaks at 31.2 eV and 33.4 eV, corresponding to $W4f_{7/2}$ and $W4f_{5/2}$, respectively [23]. The peaks centered at 35.6 eV and 37.8 eV correspond to $W4f_{7/2}$ and $W4f_{5/2}$ attributed to WO_3 (W^{6+}) [24,25]. Figure 9(b) shows the XPS spectra of oxygen. The two main peaks of the raw data are centered at 530.7 and 531.5 eV, which are ascribed to WO_3 and to water molecules absorbed [24,25] by the film of corrosion products on tungsten immersed in the NaCl solution.

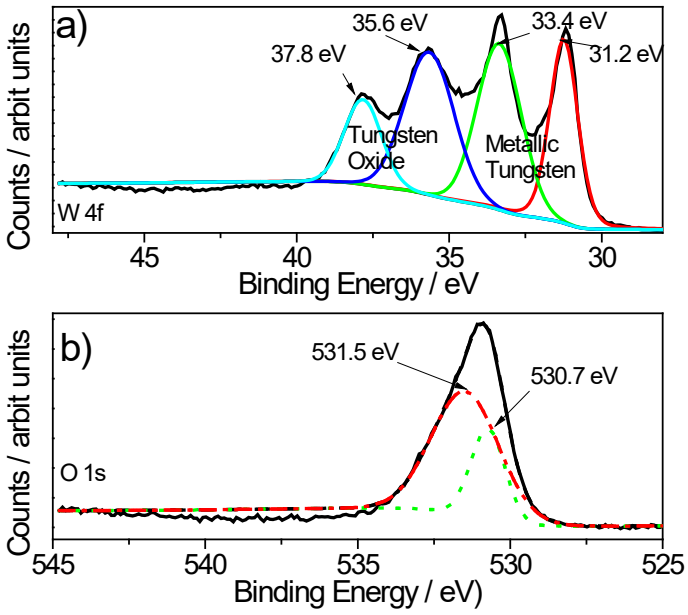

Figure 9. High resolution XPS a) W 4f and b) O 1s spectra of the protective film on tungsten (W-P) after polarization test in 3.5 wt.% NaCl (pH 6.8).

Surface analysis of tungsten/rare earth element alloys

Peaks ascribed to W and WO_3 are found in the XPS spectra of all tungsten/rare earth element alloys (Figures 10(a), 11(a), and 12(a)), as expected since W is the major component in the binary alloys.

Oxygen: The peak corresponding to O 1s for all binary alloys (Figures 10(c), 11(c), and 12(c)), was deconvoluted into two components, which were close to 530 eV and 531 eV. The peak at approximately 530 eV is commonly ascribed to metal oxides such as WO_3, La_2O_3, Ce_2O_3, CeO_2, or

ThO_2. The peak at 531 is attributed to absorbed water or hydroxide species. Observe that signal around 530 eV correspond to the metal oxides for the alloys W-2Th, W-2Ce, W-2La, and is slightly higher than that found on W-P.

Thorium: The XPS spectra measured on the surface of the W-2Th alloy after exposure to the NaCl solution are depicted in Figure 10(b). Two peaks are observed at 343.7 and 334.4 eV corresponding to the photoelectronic lines of $4f_{5/2}$ and $4f_{7/2}$ of spin-orbit 4f [26]. The peak separation between the peaks is 9.3, which agrees with the value reported elsewhere [26]. The peak binding energies and separation confirm the presence of ThO_2 in the WO_3 film formed on the surface of the W-2Th alloy.

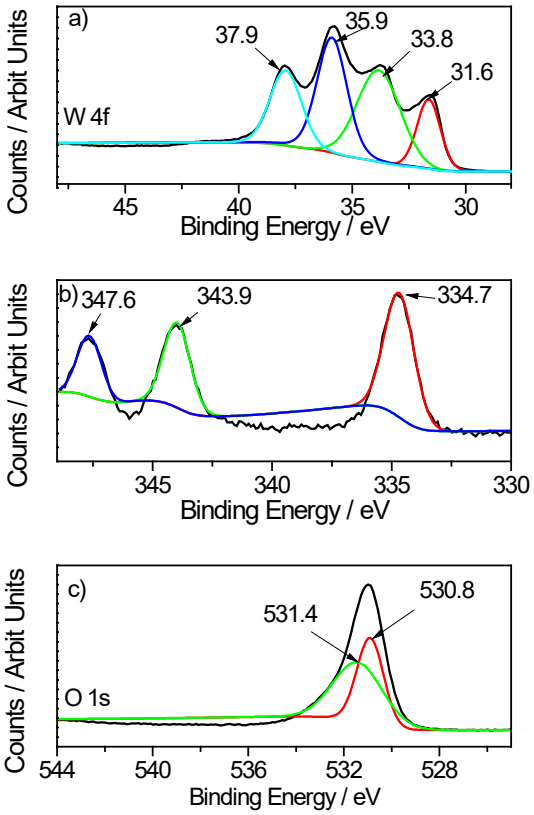

Figure 10. High resolution XPS a) W 4f, b) Th 4f, and c) O 1s spectra of the protective film on Thorium added tungsten (W-2Th) after polarization test in 3.5 wt.% NaCl (pH 6.8).

Cerium: CeO_2 and Ce_2O_3 have complex electronic structures, [27,28] which make the XPS spectra Figure 11(b), of these oxides unique. The strong satellite peaks at approximately 885.7 eV and 904.2 eV are attributed to Ce^{3+} bonding in Ce_2O_3, while the satellite peaks at approximately 882.1 and 900.4 are associated with Ce^{4+} bonding in CeO_2 [28,29]. Therefore, the deconvolution of the spectra demonstrates that both Ce_2O_3 and CeO_2 oxides coexist in the WO_3 layer.

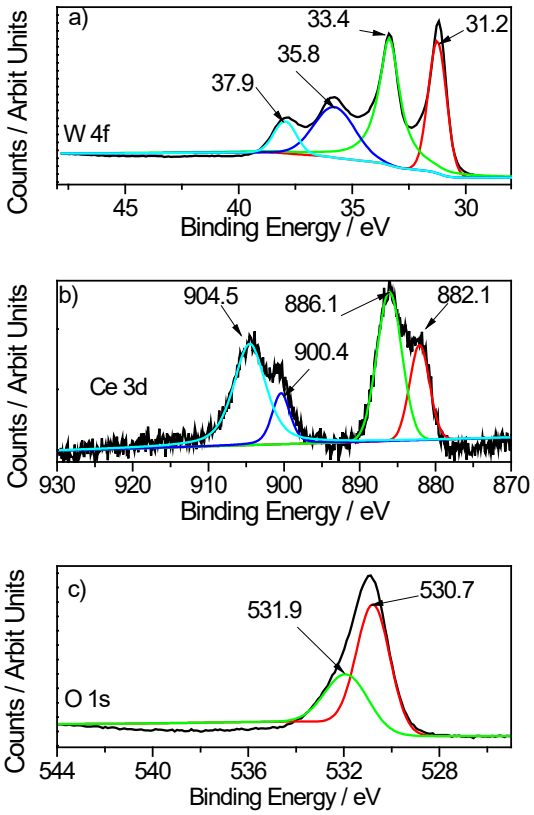

Figure 11. High resolution XPS a) W 4f, b) Ce 3d, and c) O 1s spectra of the protective film on Cerium added tungsten (W-2Ce) after polarization test in 3.5 wt.% NaCl (pH 6.8).

Lanthanum: The XPS spectra of the W-2La alloy are shown in Figure 12(b), which confirm the presence of La2O3 (La^{3+}) on the surface of the W-2La alloy [30]. This is supported by the binding energies at 835.2 eV, 838.9 eV corresponding to La $3d_{5/2}$, and 852.2 eV corresponding to La $3d_{3/2}$ [30,31].

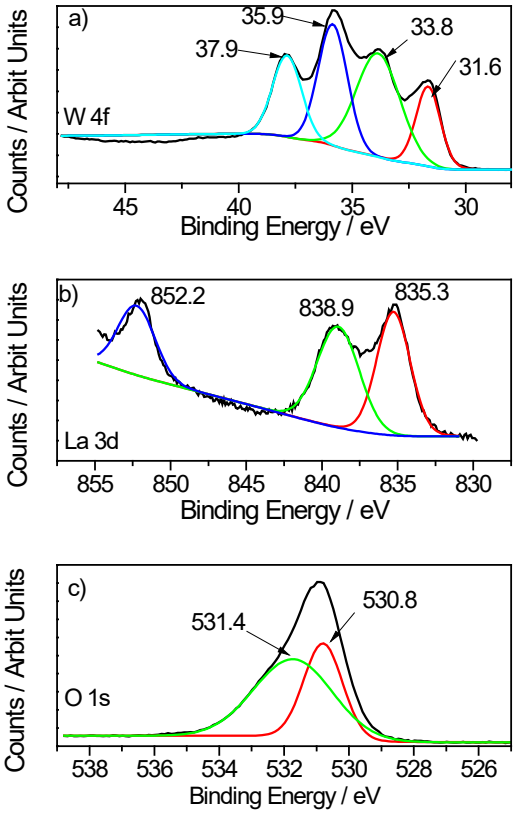

Figure 12. High resolution XPS a) W 4f, b) La 3d, and c) O 1s spectra of the protective film on Lanthanum added tungsten (W-2La) after polarization test in 3.5 wt.% NaCl (pH 6.8).

Conclusions

The corrosion of tungsten and tungsten alloys (W-2Ce, W-2Th, and W-2La) has been studied using potentiodynamic polarization and electrochemical impedance spectroscopy in 3.5 wt. % NaCl. From the results, the following conclusions can be drawn:

- The corrosion behavior of tungsten with 2 wt.% Th, Ce, or La is dominated by the corrosion properties of tungsten itself.
- Although the presence of rare earth elements has a negligible effect on the corrosion of tungsten, an observable increase in corrosion resistance is seen due to the presence of lanthanum and cerium. Also, these two alloys present a passive region on the anodic branch of the polarization curve.
- The results suggest that thorium could be replaced by non-radioactive cerium or lanthanum to improve corrosion resistance.
- The presence of an oxide film on tungsten and its dissolution at higher overpotentials were revealed by polarization and impedance measurements in a 3.5 wt.% NaCl solution and confirmed by X-ray photoelectron spectroscopy surface analysis.

Acknowledgments

The authors would like to express their gratitude to the CONACYT for providing the equipment necessary to carry out the present study through the infrastructure project under grant 205050. They would also like to thank the National Laboratory for the Study of Nano and Biomaterials (LANNBIO) at CINVESTAV-Mérida for their support. The authors would also like to thank Ing. Gualdemar Casanova for his assistance in the metallographic preparation of the samples. Vega-Lizama would like to acknowledge the CONACYT/MEXICO for her postdoctoral fellowship (BP-PA-20220718214010901-2840985).

References

[1] Shen L, Li X, Lindberg D, Taskinen P. Tungsten extractive metallurgy: A review of processes and their challenges for sustainability. Miner Eng 2019;142:1–14. doi:10.1016/j.mineng.2019.105934.

[2] Snead LL, Hoelzer DT, Rieth M, Nemith AAN. Refractory Alloys: Vanadium, niobium, molybdenum, tungsten. In: G. Robert Odette, Steven J. Zinkle, editors. Structural Alloys for Nuclear Energy Applications. Elsevier, 2019. pp. 585–640. doi:10.1016/B978-0-12-397046-6.00013-7.

[3] Wang F, Zhang X, Deng H. A comprehensive study on electrochemical polishing of tungsten. Appl Surf Sci 2019;475:587–597. doi:10.1016/j.apsusc.2019.01.020.

[4] Cordeiro CA, Sias A, Koster T, Westerink BHC, Cremers TIFH. In vivo “real-time” monitoring of glucose in the brain with an amperometric enzyme-based biosensor based on gold coated tungsten (W-Au) microelectrodes. Sensors Actuators, B Chem 2018;263:605–613. doi:10.1016/j.snb.2018.02.116.

[5] Schuster BE, Roszell LE, Murr LE, Ramirez DA, Demaree JD, Klotz BR, Rosencrance AB, Dennis WE, Bao W, Perkins EJ, Dillman JF, Bannon DI. In vivo corrosion, tumor outcome, and microarray gene expression for two types of muscle-implanted tungsten alloys. Toxicol Appl Pharmacol 2012;265:128–138. doi:10.1016/j.taap.2012.08.025.

[6] Peuster M. Biocompatibility of corroding tungsten coils: in vitro assessment of degradation kinetics and cytotoxicity on human cells. Biomaterials 2003;24:4057–4061. doi:10.1016/S0142-9612(03)00274-6.

[7] Patrick E, Orazem ME, Sanchez JC, Nishida T. Corrosion of tungsten microelectrodes used in neural recording applications. J Neurosci Methods 2011;198:158–171. doi:10.1016/j.jneumeth.2011.03.012.

[8] Idil AS, Donaldson N. The use of tungsten as a chronically implanted material. J Neural Eng 2018;15:1–13. doi:10.1088/1741-2552/aaa502.

[9] Zhao M, Zhou Z, Ding Q, Zhong M, Arshad K. Effect of rare earth elements on the consolidation behavior and microstructure of tungsten alloys. Int J Refract Met Hard Mater 2015;48:19–23. doi:10.1016/j.ijrmhm.2014.07.014.

[10] Zhang FF, Yang JC, Huang L. Research and Application of Rare Earth Tungsten Electrode Materials. Mater Sci Forum 2016;847:65–71. doi:10.4028/www.scientific.net/MSF.847.65.

[11] Bekhiti D, Creus J, Mesrati N, Abdi A, Messaoudi H. Improvement of the corrosion behavior of aluminum alloy 6061-T6 with yttrium and lanthanum conversion coatings. Mater Tehnol 2018;52:329–334. doi:10.17222/mit.2017.160.

[12] Wang C, Zhu S, Jiang F, Wang F. Cerium conversion coatings for AZ91D magnesium alloy in ethanol solution and its corrosion resistance. Corros Sci 2009;51:2916–2923. doi:10.1016/j.corsci.2009.08.003.

[13] Pourbaix M. Atlas of electrochemical equilibria in aqueous solutions. 2nd Ed. Houston, Texas: NATIONAL ASSOCIATION OF CORROSION ENGINEERS, 1974.

[14] Lyon SB. Corrosion of Tungsten and its Alloys. Shreir's Corrosion. Elsevier, 2010. pp. 2151–2156. doi:10.1016/B978-044452787-5.00105-0.

[15] Wong PK, Kwok CT, Man HC, Guo D. Laser fabrication of W-reinforced Cu layers: I. Corrosion behavior in 3.5% NaCl solution and synthetic acid rain. Mater Chem Phys 2016;181:397–408. doi:10.1016/j.matchemphys.2016.06.075.

[16] McCafferty E. Validation of corrosion rates measured by the Tafel extrapolation method. Corros Sci 2005;47:3202–3215. doi:10.1016/j.corsci.2005.05.046.

[17] Guo D, Kwok CT. Effect of pH on the corrosion behavior of tungsten-copper alloys. Corros Sci 2020;177:108994. doi:10.1016/j.corsci.2020.108994.

[18] Wang D, Xiang B, Liang Y, Song S, Liu C. Corrosion control of copper in 3.5 wt.% NaCl Solution by Domperidone: Experimental and Theoretical Study. Corros Sci 2014;85:77–86. doi:10.1016/j.corsci.2014.04.002.

[19] Hsu CH, Mansfeld F. Technical Note: Concerning the Conversion of the Constant Phase Element Parameter Y0 into a Capacitance. CORROSION 2001;57:747–748. doi:10.5006/1.3280607.

[20] Anik M. Anodic reaction characteristics of tungsten in basic phosphate solutions. Corros Sci 2010;52:3109–3117. doi:10.1016/j.corsci.2010.05.037.

[21] Boukamp BA. A Linear Kronig-Kramers Transform Test for Immittance Data Validation. J Electrochem Soc 1995;142:1885–1894. doi:10.1149/1.2044210.

[22] Sow PK, Parvatalu D, Bhardwaj A, Prabhu BN, Bhaskarwar AN, Shukla A. Impedance spectroscopic determination of effect of temperature on the transport resistances of an electro-electrodialysis cell used for concentration of hydriodic acid. J Appl Electrochem 2013;43:31–41. doi:10.1007/s10800-012-0500-7.

[23] Katoh M, Takeda Y. Chemical state analysis of tungsten and tungsten oxides using an electron probe microanalyzer. Japanese J Appl Physics, Part 1 Regul Pap Short Notes Rev Pap 2004;43:7292–7293. doi:10.1143/JJAP.43.7292.

[24] Barreca D, Carta G, Gasparotto A, Rossetto G, Tondello E, Zanella P. A Study of Nanophase Tungsten Oxides Thin Films by XPS. Surf Sci Spectra 2001;8:258–267. doi:10.1116/11.20020801.

[25] Sivathas SS, Murugan S, Babu AV, Ramalingam S, Thirumurugan R, Victoria DCERB. Characterization of WO3 thin films deposited by spray pyrolysis technique and its role in gas sensing. EUREKA, Phys Eng 2022;2022:101–113. doi:10.21303/2461-4262.2022.002347.

[26] Huentupil Y, Cabello-Guzmán G, Chornik B, Arancibia R, Buono-Core GE. Photochemical deposition, characterization and optical properties of thin films of ThO2. Polyhedron 2019;157:225–231. doi:10.1016/j.poly.2018.10.023.

[27] Paparazzo E. Use and mis-use of x-ray photoemission spectroscopy Ce3d spectra of Ce2O3 and CeO2. J Phys Condens Matter 2018;30:1–38. doi:10.1088/1361-648X/aad248.

[28] Zhang J, Wong H, Yu D, Kakushima K, Iwai H. X-ray photoelectron spectroscopy study of high-k CeO2/La2O3 stacked dielectrics. AIP Adv 2014;4:1–9. doi:10.1063/1.4902017.

[29] He Q, Wang X, Zhou P, Ge Q, Fu T, Chen S, Xiao F, Yang P, He P, Jia L, Yang D. Facile one-pot synthesis of nanocoral-like cerium-activated cobalt selenide: a highly efficient electrocatalyst for oxygen evolution reaction. J Mater Sci 2021;56:20037–20049. doi:10.1007/s10853-021-06544-3.

[30] Huang X, Li N, Cao L, Zheng J. Electrodeposited lanthanum film as chromate replacement for tinplate. Mater Lett 2008;62:466–469. doi:10.1016/j.matlet.2007.05.071.

[31] Sunding MF, Hadidi K, Diplas S, Løvvik OM, Norby TE, Gunnæs AE. XPS characterisation of in situ treated lanthanum oxide and hydroxide using tailored charge referencing and peak fitting procedures. J Electron Spectros Relat Phenomena 2011;184:399–409. doi:10.1016/j.elspec.2011.04.002.